ELSEVIER

Contents lists available at ScienceDirect

Journal of Membrane Science

journal homepage: http://www.elsevier.com/locate/memsci





Supported gas membrane-based ammonia removal and recovery for a pH-dependent sink: Effect of water vapor transport

Philip A. Aligwe^a, Kamalesh K. Sirkar^{a,*}, Christian J. Canlas^b, Wu-Cheng Cheng^b

- a Otto York Department of Chemical and Materials Engineering, New Jersey Institute of Technology, University Heights, Newark, NJ, 07102, USA
- ^b W. R. Grace Catalysts Technologies, 7500 Grace Drive, Columbia, MD, 21044, USA

ARTICLE INFO

Keywords: Ammonia removal Hollow fiber membranes Mass transfer coefficient Experiments and models Strip-side pH dependence

ABSTRACT

Sometimes NH_3 is stripped from process/effluent streams through hydrophobic porous hollow-fiber-membranes (HFMs) via a supported-gas-membrane (SGM) process and recovered in concentrated H_2SO_4 solution as $(NH_4)_2SO_4$. To recover relatively purified $(NH_4)_2SO_4$, one can avoid excess H_2SO_4 with a more dilute H_2SO_4 strip solution. Neglect of strip-side mass-transfer resistance for low-pH strip H_2SO_4 solutions is not desirable with higher-pH H_2SO_4 strip solutions. Small hollow-fiber membrane modules (HFMMs) were used with a higher-pH H_2SO_4 strip solution. Mass transfer was successfully modeled using reaction-enhanced mass transport in higher-pH H_2SO_4 solution. Employing larger-scale crossflow HFMMs, time-dependent ammonia removal from a large tank having ammonia-containing process effluent was modeled for batch recirculation operation. The larger-scale modules employ shell-side feed liquid in crossflow with an overall countercurrent flow pattern and acid flow in the tube side. Modeling ammonia transport without water vapor transfer can cause substantial errors in batch recirculation method. Water vapor transport was considered here for low-pH and high-pH H_2SO_4 strip solutions for ammonia-containing feed in a large tank. Model results describe literature-based experimentally observed mass transfer behavior in industrial-treatment systems well. Model calculations were also made for continuous ammonia recovery from industrial effluents by a number of series-connected HFMMs without any batch recirculation.

1. Introduction

In a variety of effluents [1,2] causing ammonia emission, ammonia is present either as ammonium ion or as ammonia gas or as a mixture of both depending on the pH [3,4]. Conventional industrial practice involves raising the effluent pH to >11 by adding alkali to ensure that almost all of the ammonia is present as NH₃ gas and not as NH $^{\perp}$ ion, strip it with air in a packed tower and then recover it from the air as (NH₄)₂SO₄ by absorbing it in a concentrated sulfuric acid solution in a separate packed tower. Other treatment methods include ion exchange based processes [5] or biodegradation [6]; the latter is not useful for effluents having high concentrations of ammonia where it is best to recover ammonia.

In the supported gas membrane (SGM) based process, a porous hydrophobic hollow fiber membrane (HFM) is used with the volatile species-containing feed solution on one side; the stripped volatile species diffuses through the gas-filled membrane pores into an appropriate stripping solution on the other side and undergoes reabsorption. The

following stripping-reabsorption examples include:

- stripped NH₃ from a feed solution is absorbed into a low pH sulfuric acid solution on the other side producing ammonium sulfate [7–9];
- (2) acidic volatile solute HCN stripped from a feed solution is reabsorbed into a caustic solution to produce nonvolatile sodium cyanide [10,11];
- (3) ammonia is stripped from a solution containing ammonia and CO_2 for reabsorption into sulfuric acid solution [12];
- (4) volatile aliphatic amines stripped into a sulfuric acid solution [13].

Such processes using a HFM module are also known as Trans-MembraneChemiSorption (TMCS) [14]. This technique has also been investigated extensively for removing cyanide from various streams including hydrometallurgical streams where an alternate designation, gas filled membrane absorption process (GFMA), has also been used

E-mail address: sirkar@njit.edu (K.K. Sirkar).

^{*} Corresponding author.

[15–18]; these studies have also devoted efforts to design such a membrane process. Extensive experimental studies on cyanide removal by SGMs were also carried out in another group [19–23].

Large hollow fiber membrane devices with as high a surface area as 130 m² [24] are being used commercially [14] for example for ammonia removal and production of ammonium sulfate as well as for cyanide removal [16]. The mode of operation of large HFM devices in such applications can involve batch recirculation where the feed solution is in a large tank. A pump is used to push this solution from the feed tank through the HFM modules back into the feed tank whereas the concentrated sulfuric acid solution is circulated through the other side of the membrane module from another tank containing the concentrated sulfuric acid solution. In this process, one may employ 1-3 (say) HFM modules in series to remove ammonia significantly from the solution flowing through the HFM modules. An alternate continuous mode of operation [16] involves a larger number of large HFM modules connected in series to reduce the solute (e.g., ammonia, cyanide) concentration in the module effluent to levels acceptable for discharge or other uses of the liquid stream.

In either flow configurations for such treatment processes, one usually neglects the strip side mass transfer resistance [7-9,16,17] by assuming a highly concentrated sulfuric acid solution or NaOH solution as the case may be. There are two major consequences of such an assumption.

The vapor pressure of water above the concentrated sulfuric acid solution (for example) in the strip solution reservoir is much lower than that in the feed solution coming in from the feed tank. In batch recirculation, this leads to considerable water transfer from feed tank to strip tank. This process was clearly identified in the larger-scale 10x28 LiquiCel® module-based experimental study on ammonia transport reported in Ref. [24]: "The filling level shifts due to water vapor transport from the water loop to the acid loop because of the difference in water vapor pressures between the two liquid phases". To block this water transfer by osmotic distillation due to the very different osmotic pressures of the two solutions on two sides of the membrane, Shen et al. [23] raised the strip side solution temperature and initiated membrane distillation process to counter osmotic distillation. Therefore, in ammonia removal process via batch recirculation, if the temperatures of the two solutions are close, one has to account for moisture transfer from the feed solution to the strip solution with adverse consequences for removal of ammonia from the feed solution. We have developed a model here that takes into account moisture transfer in batch recirculation-based SGM process and compared model results with data from a study using two large-scale HFM modules in series [24].

Such transfer of water between two solutions having very different osmotic pressures on two sides of a membrane is encountered in liquid membrane processes with undesirable consequences. In emulsion liquid membrane processes, if the internal phase has a solution with a high osmotic pressure due to high acid or alkali concentration, water transfer from a dilute external continuous phase leads to emulsion swelling with additional consequences of diluting solute concentration in the internal phase and reduced driving force for solute extraction [25]. In supported liquid membrane (SLM) processes, an organic solvent-based liquid membrane is usually present in the support membrane pores with aqueous solutions on two sides of the membrane; when an osmotic pressure gradient exists across the membrane, liquid membrane in the support membrane pores tends to become unstable [26]; ultimately the liquid membrane is destroyed.

High concentration of sulfuric acid in the strip solution also suggests that any ammonium sulfate formed probably will have significant contamination from sulfuric acid. It is sometimes of interest to produce ammonium sulfate with a very limited contamination as well as achieve a higher effective utilization of sulfuric acid. This requires consideration of strip side resistance and determining the reduction in ammonia removal rate. This problem was investigated here experimentally; a local instantaneous reaction-enhanced mass transfer model was also

developed to describe this process. In addition, the corresponding analysis for large-scale system operation in batch recirculation mode was also developed here.

Modeling of both of these configurations for large 10x28 LiquiCel® HFM-based modules in this study employed the results from the approach of Aligwe et al. [27]. They had estimated the membrane resistance by evaluating the experimental ammonia transfer rate through membrane modules having a small amount of membrane surface area in the context of a membrane module performance model. In ammonia extraction by SGM processes via reabsorption into a low pH sulfuric acid strip solution, membrane resistance virtually controls ammonia transfer behavior in the feed liquid flowing in cross flow over the hollow fibers. Thus, membrane resistance information from Ref. [27] was integral to modeling of experimental data for high pH strip solution as well as large device modeling for both ranges of pH. Simultaneously, the analysis of Sengupta et al. [28] of the experimental data on deoxygenation from a variety of LiquiCel® modules including 10x28 ones and a result from Zheng et al. [29] were utilized in the modeling of the large-scale device, 10x28 LiquiCel® module.

2. Materials and methods

Ammonium chloride (NH₄Cl) (53.49 g/mol, \geq 99.0%, Fisher, Hanover Park, IL); potassium hydroxide (56.11 g/mol, 90.0%, Sigma, Allentown, PA). A 0.5x1 MicromoduleTM provided by 3 M (Charlotte, NC, USA) was used as the crossflow device. This device contained 700 microporous hydrophobic hollow fiber membranes. Table 1 provides information on the 0.5x1 MicromoduleTM and the much larger 10x28 LiquiCel® modules used in industrial operations.

An experimental procedure similar to that described in an earlier study [27] was followed. However, in this work, a sulfuric acid solution with a higher pH of 1.4 (± 0.2) was used for ammonia reabsorption at the strip side-membrane interface. Ammonia removal runs were made at four inlet ammonia concentrations (87, 487, 654 and 722 ppm) and four feed flow rates (7, 10, 20 and 28 ml/min). The setup used for the removal via a 0.5×1 MicroModuleTM is shown in Fig. 1.

Ammonium chloride (NH_4Cl) solution was prepared by dissolving a certain amount of the salt in deionized water. Afterwards, 4 M KOH was added to increase the solution pH to 12. This feed solution was fed over the outside surface of the microporous hydrophobic hollow fibers from a 5 L s steel Millipore pressure vessel. A Micropump (Ismatec BVP-Z) was used to achieve this. The sulfuric acid strip solution, in crossflow with the feed solution, was simultaneously introduced via the bores of the hollow fibers from another pressure vessel. The two solutions were

Table 1Hollow fiber membrane/module information.

Module	0.5x1 MicroModule™	10x28 LiquiCel®
Number of fibers, N	700	224,000
Porous polypropylene hollow fiber type	X-50	X-50
Effective module length, L (cm)	3	61
Effective fiber length, W (cm)	3	_
Inner/Outer radius of large cartridge,	_	5.7/12.25
R_{ci}/R_{co} (cm)		
Membrane surface area (cm ²)	99 ^c	1,300,000 ^d
Fractional open area for flow of liquid in radial	-	0.37
plane f _x		
Packing fraction of hollow fibers in the module, fp	-	0.43
Hollow Fiber Inner radius, Ri (cm)	0.011	0.011
Hollow Fiber Outer radius, Ro (cm)	0.015	0.015
Porosity,	0.4	0.4
^a Tortuosity, τ	-	-
Pore diameter, d _p (cm)	$4x10^{-6}$	$4x10^{-6}$

^a Various estimates are available.

^c Calculated

 $^{^{\}rm d}$ Module data sheet; hollow fiber ends potted with epoxy in the tube sheet in the MicroModule $^{\rm TM}\!.$

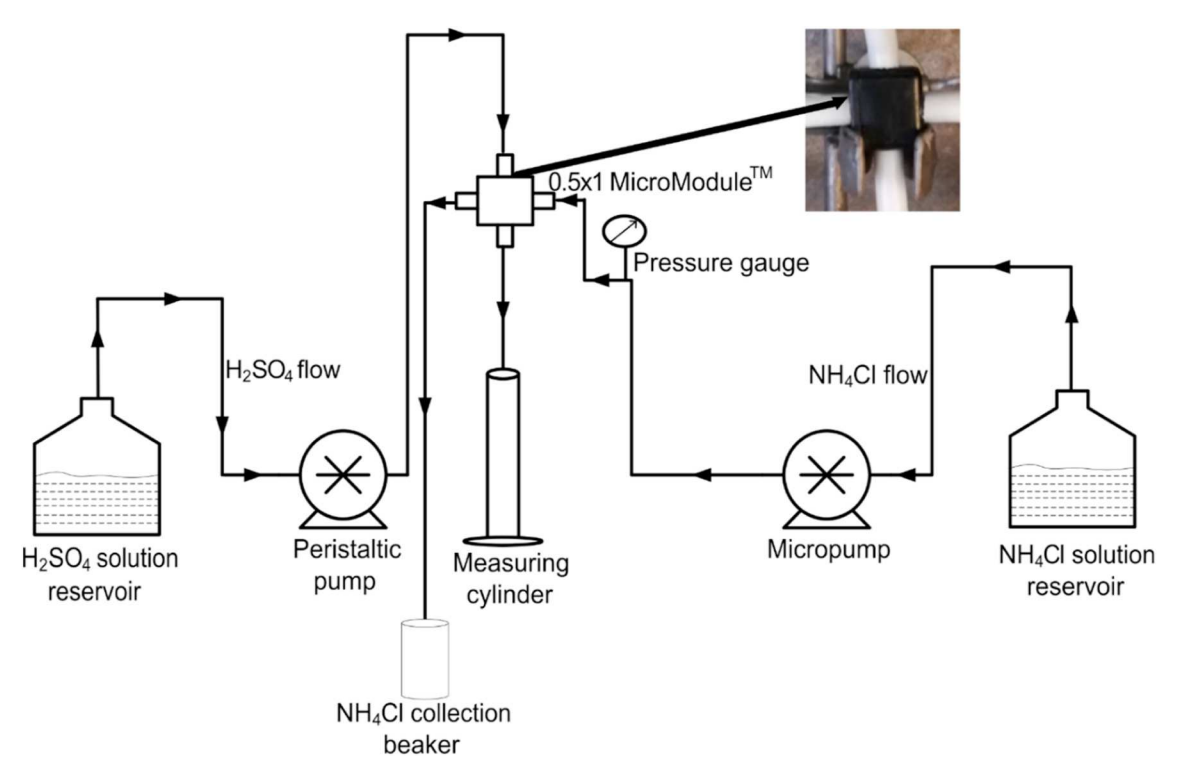


Fig. 1. Schematic of ammonia removal experiments conducted in 0.5x1 MicroModuleTM (adapted from Refs. [27]).

passed in once-through fashion (Fig. 1). The tubings used were selected based on the pump-heads (Masterflex 7518-60 and 77201-62) and resistance to the chemicals intended to be passed through them.

Further, a pH meter (Orion Star A212, The Lab Depot, Dawsonville, GA) was used to determine the pH levels of the feed and strip solutions. The pH probe was calibrated between -0.91 and 14 using three buffer solutions provided by the manufacturer as well as sulfuric acid and sodium hydroxide standards prepared in the laboratory. A high-performance ammonia gas ion selective electrode (Orion 9512HPBNWP, Fisher, Hanover Park, IL) was used to measure the ammonia concentration in the samples. Electrode calibrations were performed before each run, and NH₃ concentration values were displayed in ppm unit on the connected meter.

3. Modeling of ammonia transport in various SGM modules

3.1. Micromodule

The differential mass balance in one fiber layer is defined in terms of the feed volumetric flow rate Q, and the overall mass transfer coefficient, K_o , via the following equation [28]:

$$-Q dC = K_o dA_T C$$
 (1)

Further, the transfer area, dA_T , is expressed in terms of the outer diameter of one hollow fiber d_F , and fiber length perpendicular to the feed solution in crossflow, W [28],:

$$dA_T = \pi d_F W \frac{N}{n_f} \tag{2}$$

where n_f is the total number of fiber layers and N is the total number of hollow fibers. Combining equation (1) with equation (2) and integrating with respect to the inlet and outlet ammonia concentrations, C_o and C_{out} respectively, we obtain equation (3):

$$\ln\left(\frac{C_o}{C_{out}}\right) = \frac{K_o \, \pi d_F W N}{Q} \tag{3}$$

In mass transfer modeling, the overall mass transfer coefficient of a transferring species is generally expressed using a resistances-in-series approach. For ammonia gas transfer studies performed with hollow fiber membrane modules, three resistances due to the liquid film on the feed side $(1/k_f)$, the membrane $(1/k_m)$ and the sulfuric acid strip side $(1/k_s)$ have been reported [8,9,12,13].Hence, the overall mass transfer coefficient of ammonia, K_o , via hollow fiber modules is given by the following relationship:

$$K_o = \frac{1}{\frac{1}{k_f} + \frac{1}{k_m} + \frac{1}{k_s^* \varphi}} \tag{4}$$

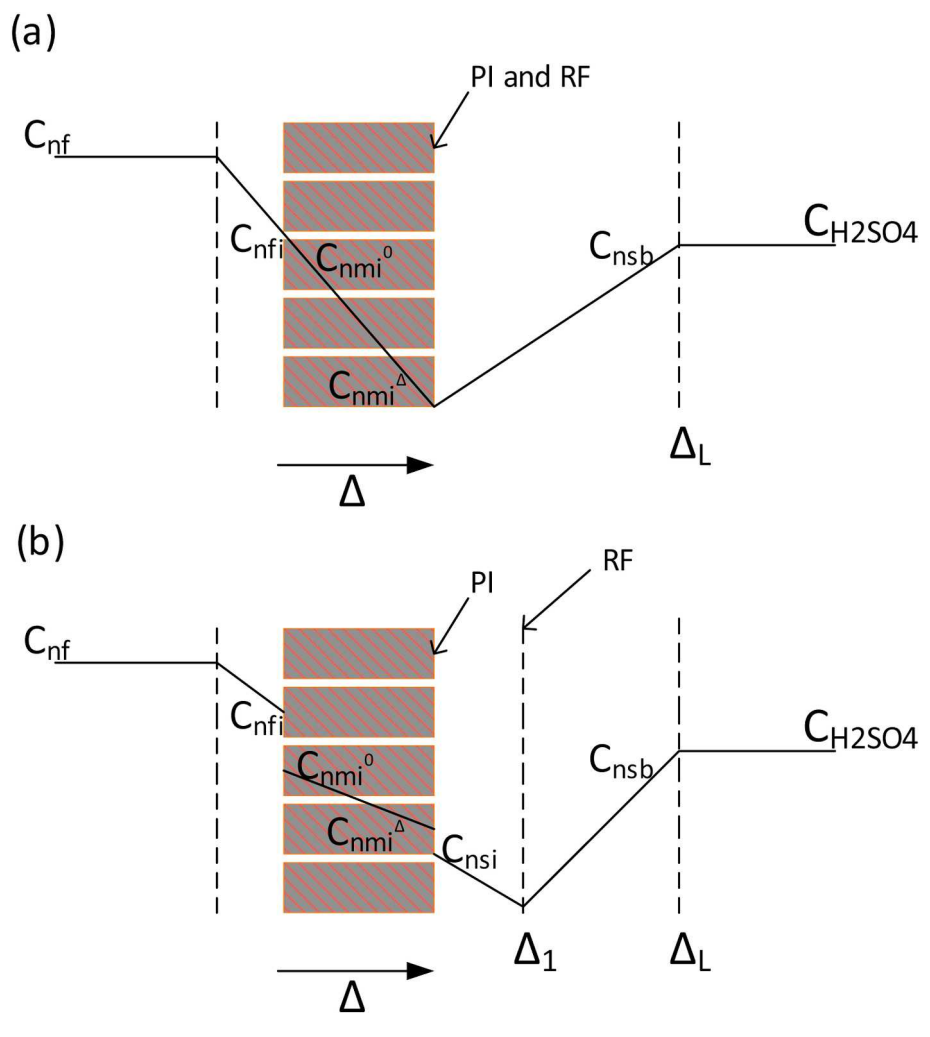
where φ , the enhancement factor, is a parameter that accounts for the contribution of the reaction between ammonia and sulfuric acid at the strip side-membrane interface to the strip side mass transfer coefficient (i.e., k_s). For high H₂SO₄ pH system, k_s has a finite value which can be explained by the presence of a phase interface (PI) which is distinct from the reaction front (RF), as illustrated in Fig. 2.

3.1.1. Feed side mass transfer coefficient of NH₃

Generally, Sherwood number of a flowing liquid is correlated with the Reynolds number and the Schmidt number via an equation of the following form:

$$\frac{k_f d_F}{D_i} = a \left[\frac{d_F v_x \rho_{NH3}}{\mu} \right]^b \left[\frac{\mu \rho_{NH3}^{-1}}{D_{NH3,L}} \right]^c$$
 (5)

Equation (5) can be rewritten as relation (6a) in the form of the feed side mass transfer coefficient, k_f correlated to a composite transport property parameter, Λ , and the local axial velocity on the shell side at distance x (shown in Fig. 3), ν_x : where ν_x and Λ are defined as follows:



 $\textbf{Fig. 2.} \ \ \text{Concentration profiles of NH}_{3} \ \text{transfer via a hollow fiber membrane to (a) low pH H}_{2}\text{SO}_{4} \ \text{strip solution and (b) high pH H}_{2}\text{SO}_{4} \ \text{strip solution.}$

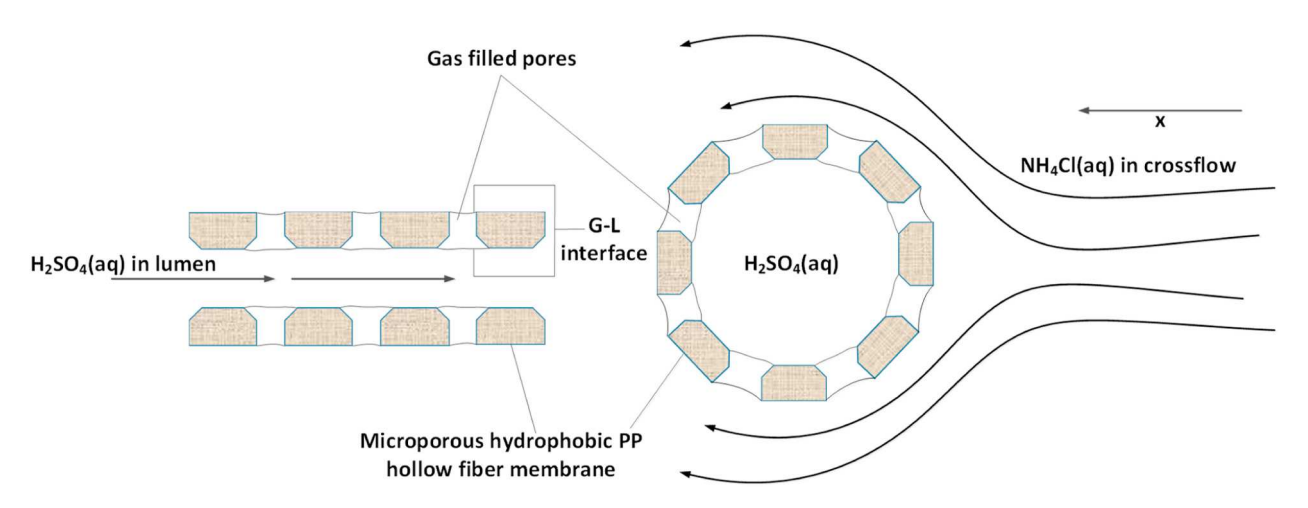


Fig. 3. Crossflow of ammonium chloride (NH₄Cl) feed solution around one hollow fiber in a 0.5x1 MicroModuleTM. G-L stands for gas-liquid (adapted from Refs. [27]).

 $k_f = \Lambda v_x^b \tag{6a}$

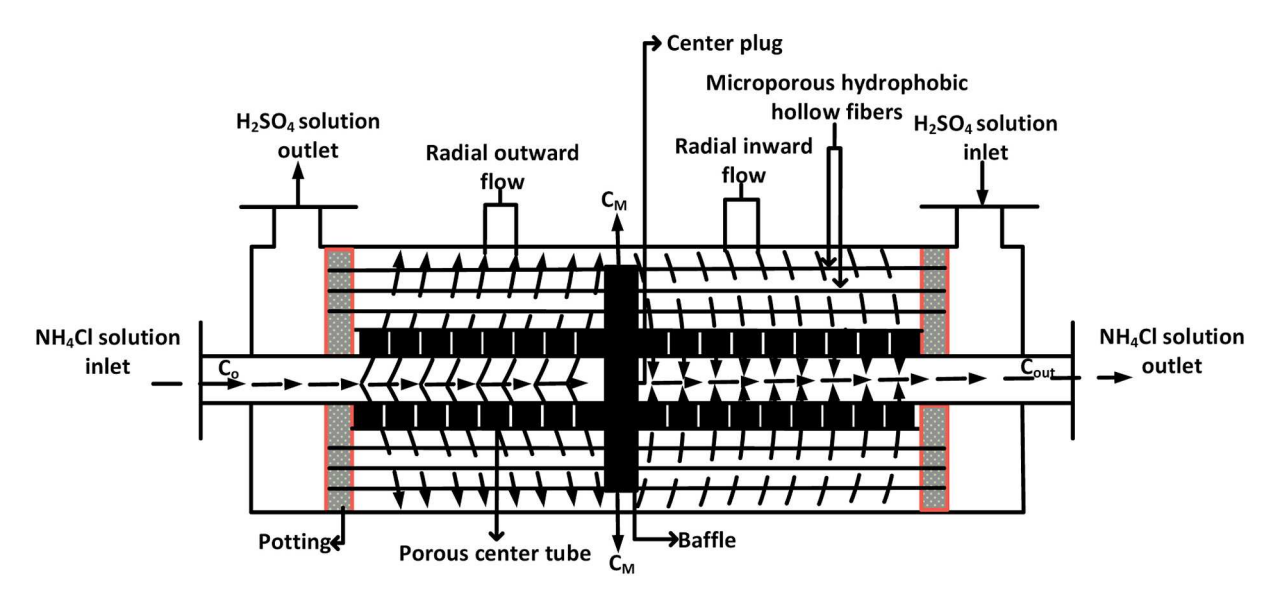


Fig. 4. Schematic for flow directions of two streams in a single 10x28 LiquiCel® hollow fiber module with two zones on two sides of the central baffle (adapted from Ref. [27]).

$$v_x = \frac{Q_x}{A_{fc}} ; \Lambda = \frac{a}{d_F^{1-b}} \left[\frac{\rho}{\mu} \right]^{b-c} [D_{NH3,L}]^{1-c}$$
 (6b)

3.1.2. Membrane mass transfer coefficient of NH₃

The membrane mass transfer coefficient, k_m , can be expressed in terms of the vapor phase diffusion coefficient of ammonia, $D_{NH3,g}$, and the effective Henry's constant H_{eff} [12]:

$$k_{m} = \frac{D_{NH3,g} * \left(\frac{\varepsilon}{\tau}\right)_{*} H_{eff}}{R_{i} \ln(R_{o}/R_{i}) RT}$$
(7a)

Since the membrane pore diameter (d_p) is less than 10^{-7} m, the membrane diffusion coefficient is the same as the Knudsen diffusion coefficient:

$$D_{NH_{3,g}} \approx D_{g,k} = \frac{d_p}{3} \sqrt{\frac{8RT}{\pi M}}$$
 (7b)

The relationship between the effective Henry's constant H_{eff} and Henry's constant H is given by relation (7c) [3]:

$$Log_{10}(H_{eff}/H) = hI \tag{7c}$$

where,

$$h = h_{+} + h_{-} + h_{G}$$
 (8a)

and the ionic strength I is given by

$$I = \frac{1}{2} \sum C_i z_i^2 \tag{8b}$$

3.1.3. Strip side mass transfer coefficient of NH₃

Since the strip solution is flowing through the hollow fiber bore, the strip side mass transfer coefficient over a length L can be described by Leveque solution [30]:

$$k_s = \frac{1.077 \, D_{NH3,L}^{2/3} d_i^{-1/3} v^{1/3}}{L^{1/3}} \tag{9}$$

3.1.4. Enhancement factor

The enhancement factor φ for k_s in an instantaneous acid-base reaction is given by [30].

$$\varphi = 1 + \frac{D_{H2SO4,L} * C_{H2SO4} * a_{NH3}}{D_{NH3,L} * C_{nsi} * a_{H2SO4}}$$
(10a)

The concentration of NH₃ at the strip side-membrane interface, C_{nsi} , was estimated from the experimental overall mass transfer coefficients from Ref. [27], feed concentration from this study, C_{nf} , and the strip side mass transfer coefficient, k_s , via the following relation (10b):

$$C_{nsi} = \frac{K_o * C_{nf}}{k_-} \tag{10b}$$

Combining equations (3), (4), (6a) and (6b), the inlet to outlet concentration ratio $\left(\frac{C_0}{C_{out}}\right)$ can be rewritten in terms of feed volumetric flow rate and composite transport property parameter, Λ :

$$\ln\left(\frac{C_o}{C_{out}}\right) = \pi d_F W N \begin{bmatrix} 1 \\ \frac{A_F^b}{A} \frac{Q^{1-b}}{A} + \frac{Q}{k_m} + \frac{Q}{k_s^* \varphi} \end{bmatrix}$$
 (11)

The ammonia separation efficiency E can be defined in terms of C_o and C_{out} by the following equation:

$$E = 1 - \frac{C_{out}}{C_{out}} \tag{12}$$

Therefore, equation (11) can be rewritten to describe the separation efficiency in terms of the feed volumetric flow rate:

$$\ln\left(\frac{1}{1-E}\right) = \pi d_F W N \begin{bmatrix} 1\\ \frac{A_{fc}^b Q^{1-b}}{\Lambda} + \frac{Q}{k_m} + \frac{Q}{k_s^* \varphi} \end{bmatrix}$$
(13a)

The overall mass transfer coefficient K_0 can be expressed in terms of the ammonia separation efficiency as follows:

$$K_o = \frac{Q}{A_T} \ln \left(\frac{1}{1 - E} \right) \tag{13b}$$

3.2. 10x28 industrial module

In this section a model which describes the behavior of NH₃ transport via an industrial scale module is presented. *A resistances-in-series approach being valid regardless of module dimensions is also utilized for*

this scale. Two cases are presented based on the pH of the $\rm H_2SO_4$ based stripping stream. Further, a tank balance is coupled to the model in order to represent a typical industrial process [24] which used two modules in series with the solution from tank used as feed to the modules; exiting solution is returned to the tank. This is essentially batch recirculation mode of operation.

3.2.1. Case 1: NH_3/W ater vapor transfer from the feed side to a low pH strip side

The differential equation for molar balance of actively transferring vapor species, NH_3 , over a membrane area dA_T is given by

$$Q\frac{dC_M}{dA_T} + C_M \frac{dQ}{dA_T} = -K_o C_M \tag{14}$$

where, C_M represents the concentration of ammonia at the mid-zone of the contactor. From.

Sengupta et al. [28], the number of hollow fibers inside a differential slice dN can be written in terms of the hollow fiber packing fraction f_p as follows (Table 1 provides f_p value):

$$dN = \frac{f_p 2\pi r \, dr}{\frac{\pi d_F^2}{2}} = \frac{8f_p}{d_F^2} r \, dr \tag{15a}$$

Considering one zone of the two-zone contactor, the corresponding mass transfer area, dA_T based on the hollow fiber OD, d_F , is given by:

$$dA_T = \frac{\pi d_F L \, dN}{2} \tag{15b}$$

Now $\frac{dQ}{dA_T}$ in equation (14) represents the liquid phase volume flux of water which is essentially determined by the water vapor mass transfer coefficient K_{H_2O} and its partial pressure difference between the feed and strip side $(P_f - P_e)$:

$$\frac{dQ}{dA_T} = -K_{H_2O} * (P_f - P_s) * \frac{MW_{H_2O}}{\rho_{H_2O}}$$
 (16a)

The vapor phase mass transfer coefficient of water being transferred through a porous membrane of thickness δ can be expressed in terms of its Knudsen diffusion coefficient, D_{kHDO} :

$$K_{H_2O} = \frac{D_{H_2O,k} * \left(\frac{\varepsilon}{\tau}\right)}{\delta RT} \tag{16b}$$

Due to high strip side H_2SO_4 concentration, feed side water vapor pressure is much higher than that of the strip side (i.e., $P_f \gg P_s$). Thus, the result of such an assumption is given by (17):

$$Q\frac{dC_{M}}{dA_{T}} = -C_{M} \left[K_{o} - \left(K_{H_{2}O} P_{f} * \frac{MW_{H_{2}O}}{\rho_{H_{2}O}} \right) \right]$$
(17)

The product, $K_{H_2O}P_f*\frac{MW_{H_2O}}{\rho_{H_2O}}$ is essentially the "liquid" phase volume flux of water, K'_{H_2O} .

Combining (15a), (15b) and (17), an expression that describes C_M in terms of the individual mass transfer coefficients of ammonia and the "liquid" phase volume flux of water is obtained as:

$$\frac{dC_M}{C_M} = \frac{-4\pi f_p L}{d_F Q} \left| \frac{1}{\frac{1}{k_f} + \frac{1}{k_m} + \frac{1}{k_s *_{\varphi}}} - K'_{H_2 O} \right| r dr$$
 (18a)

Expressions for k_f and k_m are given in Ref. [27]; however, at low pH, $\frac{1}{k_s} \approx 0$. Integrating both sides for one zone of the contactor, relation (18b) is obtained:

$$\int_{C_o}^{C_M} \frac{dC_M}{C_M} = -\int_{R_{Ci}}^{R_{Co}} \frac{4\pi f_p L}{d_F} \left| \frac{1}{\frac{(\pi f_s L)^b r^b Q^{1-b}}{\Lambda} + \frac{Q}{k_m}} - \frac{K_{H_2O}}{Q} \right| r dr$$
 (18b)

 C_M can be replaced with C_{out} , assuming only one zone is being considered in the integration procedure. Thus, the following expression is obtained:

$$ln\left(\frac{C_o}{C_{out}}\right) = I_1 = \frac{4\pi f_p L}{d_F} \int_{R_{Ci}}^{R_{Co}} \left[\frac{1}{\frac{(\pi f_x L)^b r^b Q^{1-b}}{\Lambda} + \frac{Q}{k_m}} - \frac{\dot{K}_{H_2 Q}}{Q} \right] r dr$$
 (18c)

Hence, for one module (*with* two zones), C_{out} can then be expressed in terms of C_o as follows:

$$C_{out} = C_o \exp(-2I_1) \tag{18d}$$

Similarly, for two modules in series:

$$C_{out} = C_o \exp(-4I_1) \tag{18e}$$

3.2.1.1. Tank balance I (water vapor loss). Given feed tank volume V at any time t, equation (19a) provides a differential equation for molar NH $_3$ concentration in the tank, C_t :

$$V\frac{dC_t}{dt} + C_t\frac{dV}{dt} = -(Q_{in}C_t - Q_{out}C_{out}) = -G$$
(19a)

where G signifies the rate of NH $_3$ transfer via the two external membrane modules, and,

$$\frac{dV}{dt} = -Q_{loss} \tag{19b}$$

describes the volume rate of water loss from the feed tank.

Similar to (18e), C_{out} can also be expressed in terms of C_t as follows:

$$C_{out} = C_t \exp(-4I_1) \tag{20}$$

V can now be expressed in terms of the initial tank volume V_o and time t using the following relationship:

$$V = V_o - Q_{loss}t \tag{21}$$

Combining (19a), (19b), (20) and (21) and integrating both sides, the following expression for C_t is obtained in terms of the initial feed concentration C_0 :

$$C_t = C_o \exp\left(\frac{X}{Q_{loss}} * (\ln|V_o| - \ln|V_o - Q_{loss}t|)\right)$$
(22a)

where

$$X = [(Q_{in} - Q_{loss}) \exp(-4I) - Q_{in} + Q_{loss}]$$
 (22b)

and,

$$Q_{loss} = \dot{K_{H_2O}}^* A_T \tag{22c}$$

3.2.2. Case 2: No water vapor transfer from the feed side to a high pH strip side

The water vapor pressure can be described as a function of the pH of the H_2SO_4 solution [31]. At high pH levels, the water vapor pressure on the strip side becomes equal to that of the feed. Also, as stated in Section 3.1, $\frac{1}{k} \neq 0$ and can be described by relation (9).

Considering these assumptions, relation (18c) is modified to relation (23a):

$$ln\left(\frac{C_o}{C_{out}}\right) = I_2 = \frac{4\pi f_p L}{d_F} \int_{R_{Ci}}^{R_{Co}} \left| \frac{1}{\frac{(\pi f_s L)^b r^b Q^{1-b}}{\Lambda} + \frac{Q}{k_m} + \frac{Q}{k_s^* \varphi}} \right| r dr$$
 (23a)

Similarly, C_{out} can be expressed in terms of C_o , for two modules in series:

$$C_{out} = C_o \exp(-4I_2) \tag{23b}$$

3.2.2.1. Tank balance II (no water vapor loss). A similar process analysis is followed in developing a tank balance for high H_2SO_4 side pH systems. In this case, since $Q_{loss}=0$, $Q_{in}=Q_{out}$. In addition, the tank volume is fixed over time as represented by relation (24):

$$V\frac{dC_t}{dt} = -Q_{in}(C_t - C_{out}) = -G$$
(24)

Combining (23b) and (24) and integrating the differential equation, a similar exponential function (through I_2) for C_t in terms of C_0 is obtained:

$$C_t = C_o \exp\left(\frac{t}{uV}\right) \tag{25a}$$

where,

$$u = Q_{in}(\exp(-4I_2) - 1)$$
 (25b)

4. Results and discussion

4.1. MicroModuleTM

4.1.1. Experimental results

In the previous study [27], ammonia separation efficiency through a MicroModuleTM was plotted in terms of -ln(1-E) as a function of the feed volumetric flow rate, under low strip pH conditions (see Fig. 4). The same relationship was investigated under higher strip pH conditions. These results are represented in Fig. 5. Further, the dependence of experimental overall mass transfer coefficient on the feed volumetric flow rate has also been plotted in terms of K_0 versus Q_{in} in Fig. 6. Based on a given feed volumetric flow rate, the corresponding overall mass transfer coefficient was calculated via (13b). Generally, ammonia separation efficiency increased with decreasing feed flow rates, due to longer "residence time" of the bulk feed solution in the module.

However, at the same feed flow rate, the separation efficiencies at low sulfuric acid pH conditions were higher than those investigated at higher strip side pH environment. The rationale behind this is the presence of a gas-liquid phase interface (PI) that is distinct from the reaction front (RF) resulting in a concentration boundary layer in the strip side at higher pH. In other words, ammonia reacts instantaneously

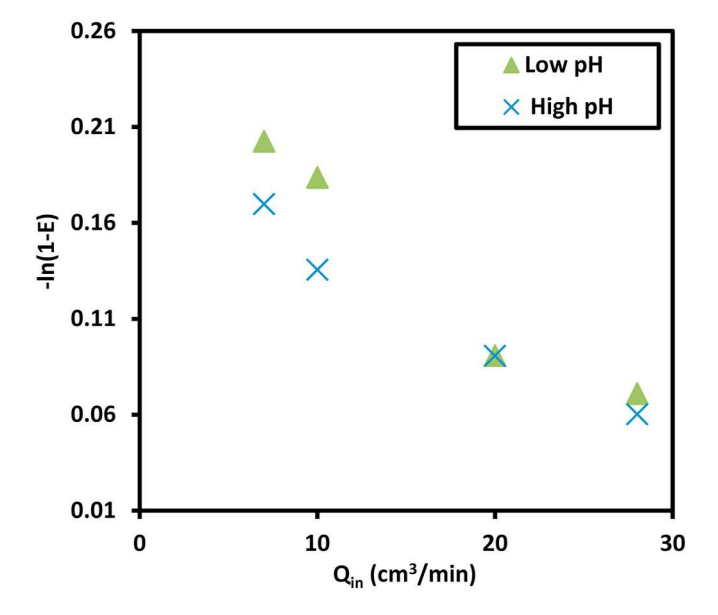


Fig. 5. Effect of feed flow rate on NH_3 separation efficiency in the MicroModule $^{\mathrm{TM}}.$

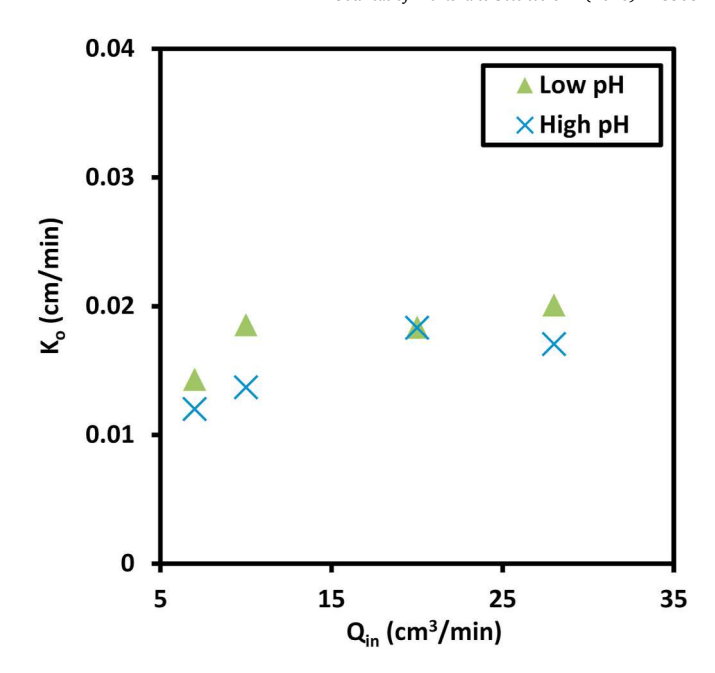


Fig. 6. Dependence of overall mass transfer coefficient on feed flow rate in the MicroModule $^{\text{TM}}$.

with sulfuric acid at the strip-side gas-liquid membrane interface at low pH values. However, at higher pH conditions, ammonia first diffuses through the PI and the boundary layer before reacting with sulfuric acid at the RF.

On the other hand, K_0 which comprises of the feed side mass transfer coefficient k_f , membrane mass transfer coefficient k_m , and strip side mass transfer coefficient k_s , increases slightly with the feed flow rate, simply due to a decrease in the boundary layer thickness of the feed liquid film in the module.

4.1.2. Modeling aspects

There are a number of unknown parameters in equations (6c), (7a) and (10a): b; the coefficient a hidden in the parameter, Λ ; the ammonia concentration at the strip side gas-liquid membrane interface, Cnsi; the membrane tortuosity, τ . In the previous study [27], given the c value of 0.33 characteristic of the transverse flow pattern in the laminar flow regime [28,29,33,34], values of a and b were estimated by applying existing shell side mass transfer correlations from literature to predict the outlet ammonia concentrations in the MicroModule $^{\text{\tiny TM}}.$ A τ value of 6.4 was estimated from the data using the equation for membrane tortuosity developed by Mackie et al. in Ref. [32]. This relationship [32] gave a better fit for outlet ammonia concentrations when plotted against the inlet concentrations via a parallel flow module also containing X-50 hollow fibers. As reported in relation (10b), a rough estimate of the ammonia concentration at the strip-side membrane interface, C_{nsi}, was calculated from experimental overall mass transfer coefficient obtained at low pH H₂SO₄ strip conditions, inlet ammonia concentrations and Leveque solution for the strip side mass transfer coefficient, k_s, given by relation (9).

From our previous study [27], b values ranged from 0.33 to 0.47, given the aforementioned tortuosity. Consequently, the predicted outlet concentrations varied by less than 5%. In this work, the same range of values were applied to predict -ln(1-E) as a function of Q. This is illustrated in Fig. 7. From the figure, the effect of b on predicted -ln(1-E) values increases with decreasing feed flow rates.

This is simply a result of increasing feed side mass transfer resistance. On the other hand, upon further investigation of predicted -ln(1-E) values (Fig. 7), the power of b was narrowed down to be between 0.45 and 0.47. Further, the mean percentage error (MPE) of the ammonia separation efficiencies calculated at various flow rate was used as a

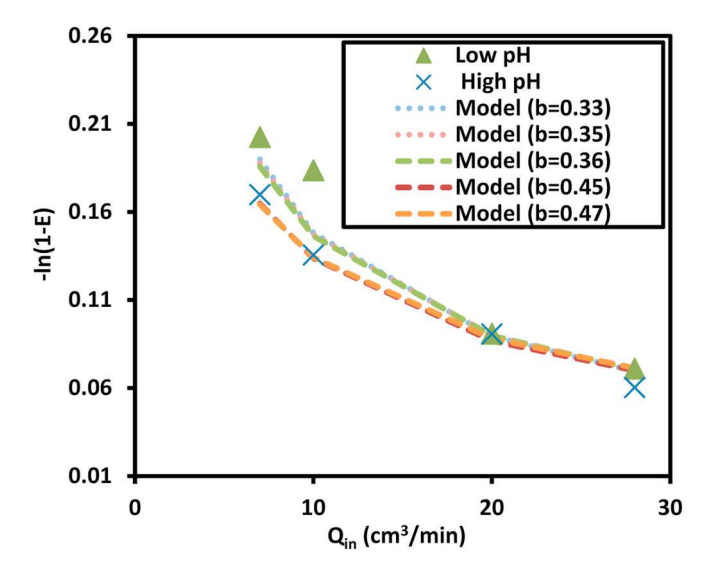


Fig. 7. Effect of power of Reynolds number (i.e., b) on predicted ammonia separation efficiencies.

means to ascertain an exact value for b. A minimum MPE was obtained at b=0.45. Hence, the film mass transfer correlation for the Micro-ModuleTM is given by the following form in (26):

$$Sh = 0.02 Re^{0.45} Sc^{0.33}$$
 (26)

4.2. 10x28 LiquiCel® industrial module

In this subsection we will analyze the results obtained from modeling an industrial scale module (10x28 LiquiCel®). No experiments were conducted with such a module in this study. However, experimental trend of data reported for ammonia removal via this module in Ref. [24] is validated here. In this study, ammonia removal via two such modules in series with the bulk feed solution being passed through the shell side and the strip solution through the tube side (both solutions are in crossflow to one another) is simulated via resistances-in-series approach. The experimental configuration in Ref. [24] was identical to this configuration. Due to the validity of this approach at this large scale [28,29], the same unknown transport parameters mentioned in the previous section applies. However, values of 'a' and 'b' were ascertained from shell-side mass transfer studies conducted in this large module in Ref. [29]: the film transfer correlation is given by equation (27):

$$Sh = 2.15 Re^{0.42} Sc^{0.33}$$
 (27)

The LiquiCel® module is built with X-50 microporous hydrophobic hollow fiber membranes which were present in the MicroModule M used in our experimental studies of ammonia removal; hence, a τ value of 6.4 was used for membrane resistance calculations [27]. The quantity C_{nsi} was estimated from ammonia feed concentration of 6000 ppm reported in Ref. [24], simulated overall mass transfer coefficients from Ref. [27] and Leveque solution for the strip side mass transfer coefficient, k_s , given by relation (9). No other parameters were involved in modeling.

Further, the system is simulated under low and high sulfuric acid pH conditions. At low sulfuric acid pH, due to partial pressure gradients of both species, water vapor is transferred along with ammonia to the strip solution [24]. The initial feed solution volume in the tank is 1 m³ [24].

The total rate of NH_3 transfer, G, as a function of feed flow rate under both types of strip side conditions is examined and illustrated in Fig. 8. Although, an increase in transfer rate with the feed flow rate through the membrane modules is expected, the flattening of the curve representing high H_2SO_4 solution pH, reflects the influence of the strip-side mass transfer resistance (i.e., $1/k_s$) on NH_3 transfer. On the other hand, water vapor transport in the low pH system may be the reason for the nearness in transfer rates at lower feed flow rates for the two cases. The

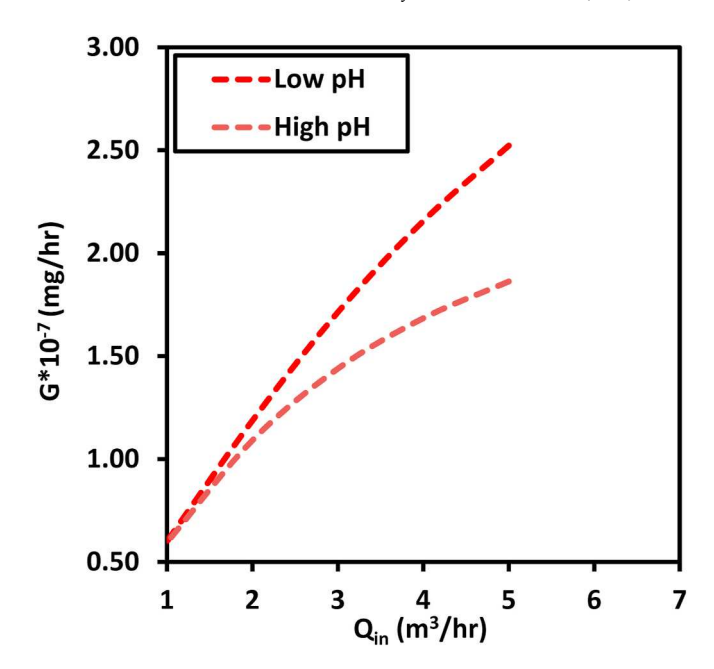


Fig. 8. Dependence of NH_3 transfer rate on feed flow rate through two membrane modules in series for two different pH values of sulfuric acid strip solutions for a feed concentration of 6000 ppm ammonia.

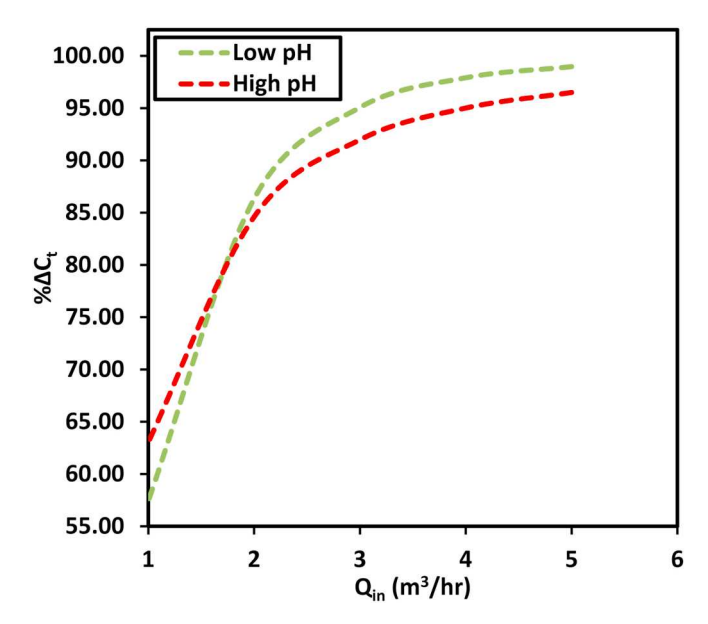


Fig. 9. Percent change in tank ammonia concentration as a function of feed volumetric flow rate simulated at an operation time of 1hr for a starting concentration of 6000 ppm.

importance of these two effects will be elaborated on in subsequent paragraphs.

In this study, a tank ammonia concentration balance is also integrated into the analytical model for two membrane modules in series in order to develop a better understanding of the industrial process performance. Ammonia concentration in the tank C_t was studied as a function of the feed flow rate in Fig. 9 and operation time t in Fig. 10 using the following two quantities describing the change in tank concentration of ammonia: $\Delta C_t = C_0 - C_t$; $\% \Delta C_t = \frac{100^+ \Delta C_t}{C_0}$.

In both systems, the percent change in tank concentration, $\%\Delta C_t$, increases with the feed flow rate through the membrane modules. This is due to increasing rates of dilution in the tank with feed flow rate at any

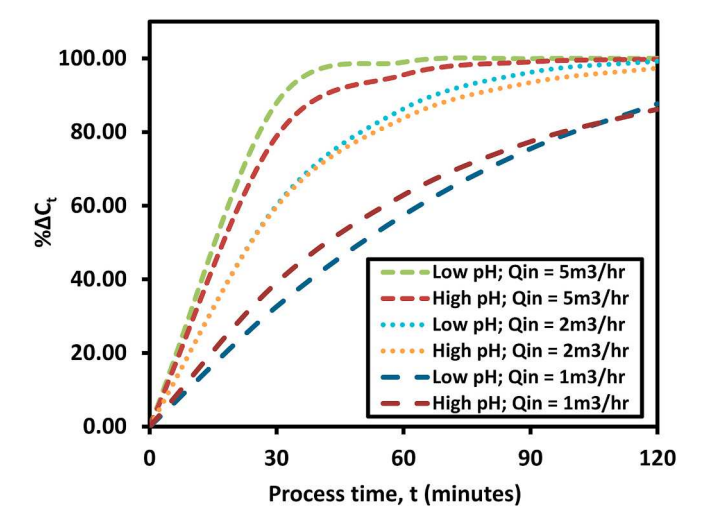


Fig. 10. Percent change in tank ammonia concentration dependence on process time simulated at feed flow rates of 1, 2 and 5 $\rm m^3/h$ for a starting concentration of 6000 ppm.

given set time. In other words, treated ammonia solution reaches the tank to 'dilute' the prior tank concentration of ammonia at a higher rate. The tank ammonia concentration decreases to a lesser extent at high $\rm H_2SO_4$ pH, due to the presence of an additional resistance on the strip side. However, this trend is reversed at the lowest feed flow rate considered (i.e., 1 m³/h). One explanation behind this phenomenon is the greater effect water vapor transport

plays at lower feed flow rates. Since water vapor transport rate remains unaffected at any given temperature by feed flow rate, under the same conditions, the net change in feed flow rate (i.e. $Q_{\rm out}/Q_{\rm in}$) increases with decreasing feed flow rates. Consequently, the actual flow rate of ammonia-containing solution ($Q_{\rm out}$) entering the tank is significantly less than 1 m³/h. Therefore, at this feed flow rate the contribution of water vapor transport counters the role of the strip side mass transfer resistance due to a higher pH.

The effect of process time on the change in tank concentration will be considered now. Further, feed flow rates considered here are 1 m³/h, 2 m³/h and 5 m³/h respectively, for both low and high sulfuric acid pH conditions. As illustrated in Fig. 10, the tank concentration changes with process time in a similar fashion discussed earlier for the feed flow rate. Generally, the change in tank concentration was expected to be higher at low pH conditions, due to negligible strip side resistance. This premise is reflected at 5 m³/h. However, at lower feed flow rates (i.e., 1 m³/h and 2 m³/h), this expectation begins to breaks down. From Fig. 10, the change in tank concentration appears to be higher at certain times at high pH conditions. Two factors namely, change in tank ammonia solution volume (ΔV_f), and the net change in the feed flow rate (Q_{out}/Q_{in}) may be contributing to these results. The former occurs as a result of water vapor loss. It is important to note that this value is essentially zero when the H₂SO₄ pH is high. As stated previously, the latter increases with decreasing flow rate. However, the trends represent coupled effects of the two factors. For instance, at a feed flow rate and simulated process time of 2 m³/h and 30 min respectively, the outlet concentration leaving the modules remains lower for the low H₂SO₄ pH system; but the extent of water vapor loss (~ 13%) leads to a significant increase in ammonia concentration in the tank. In contrast, the strip side resistance counteracts this effect at subsequent process times. This coupled effect becomes more obvious at 1 m 3 /h, where Q_{out}/Q_{in} is higher.

This relationship was also investigated with reference to the initial ammonia concentration in tank in order to compare simulated logarithmic concentration ratios (i.e., $\ln(C_0/C_t)$) illustrated in Fig. 11; this figure also includes the data reported by Ulbricht et al. [24] at 25 °C. Further, such a relationship is typically fitted with a straight line in order to ascertain the rate constant [35] or mass transfer coefficient [8] of a

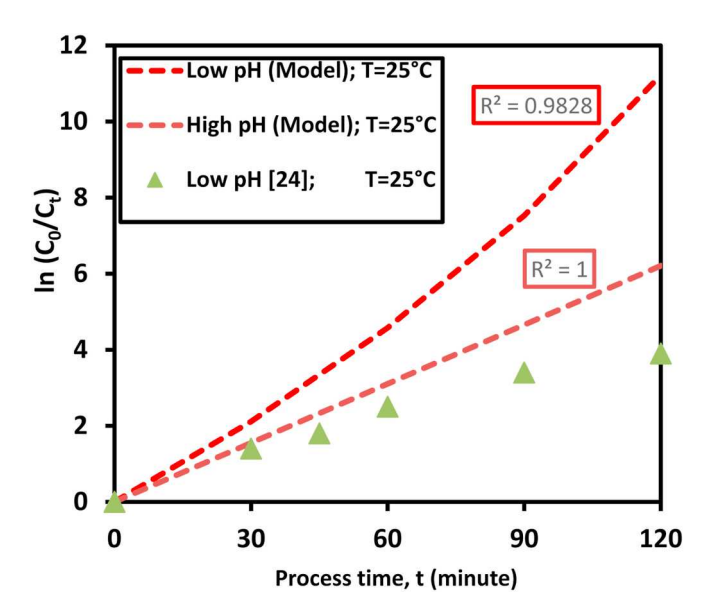


Fig. 11. Logarithmic concentration ratio in the tank as a function of process time for 6000 ppm starting concentration and $5 \text{ m}^3/\text{h}$ feed flow rate.

process. Fig. 11 indicates a perfect linear relationship between the modeled relationship at high $\rm H_2SO_4$ pH condition, whereas an excellent linearity is indicated when the strip side pH is low. The latter could be attributed to the use of feed side partial pressure of pure water (i.e., $\rm P_f$) in the simulation, which was assumed to be equal to that of pure water vapor species. A somewhat lower value which reflects the presence of other gaseous species such as, air and NH₃, tends to improve the linearity of the curve. On the other hand, concentration ratios modeled at low pH are higher in comparison to experimental results [24].

There are a variety of reasons for any discrepancy:

1) Transient water vapor partial pressure gradient in actual processes: As water vapor is transported from the NH $_3$ – containing feed to H $_2$ SO $_4$ strip solution side, the associated partial pressure gradient consequently decreases with time. Based on a calculated water vapor loss rate of 0.26 m 3 /h at room temperature, H $_2$ SO $_4$ concentration estimate (Appendix A), shows an 80% drop from the initial H $_2$ SO $_4$ concentration of 98% reported in Ref. [24]. Thus, in actual NH $_3$ removal processes via hollow fiber modules, the strip side resistance is expected to increase considerably with NH $_3$ treatment time which consequently slows down NH $_3$ transfer rates to the H $_2$ SO $_4$ strip solution. The coupled effect of water vapor transport and increase in strip side resistance leaves the feed tank solution more concentrated. The results of high pH modeling appear to be closer to those of [24].

3) Heat transfer due to reaction between NH_3 and H_2SO_4 : Heat is given off at the strip side-membrane interface when NH_3 is neutralized by H_2SO_4 ; this "excess" heat is transferred to the feed side as both solutions flow continuously via the module. This phenomena elevates the water vapor partial pressure on both sides. The extent of rise on the strip side depends on the pH of the solution. However, the data from Ref. [24] depict a more complex situation. For example, heat generated during the neutralization reaction could momentarily decrease the strip side resistance. Further, the setup in Ref. [24] had a heat exchanger on the feed tank side. The data in Ref. [24] for 32 °C appear to be closer to the high pH model results.

The overall mass transfer dependence on the feed flow rate was also investigated on this scale as shown in Fig. 12. Similar to the trend reported for the MicroModuleTM experiments and other studies [8,9,27], the simulated overall mass transfer coefficients increases slightly with the feed flow rate. In addition, due to negligible strip side resistance, the K_o values calculated for low sulfuric acid pH system are almost twice as high. On the other hand, this particular dependence affirms the validity of the current model in predicting ammonia removal processes through large scale modules. Lastly, we consider the effects of feed-side flow

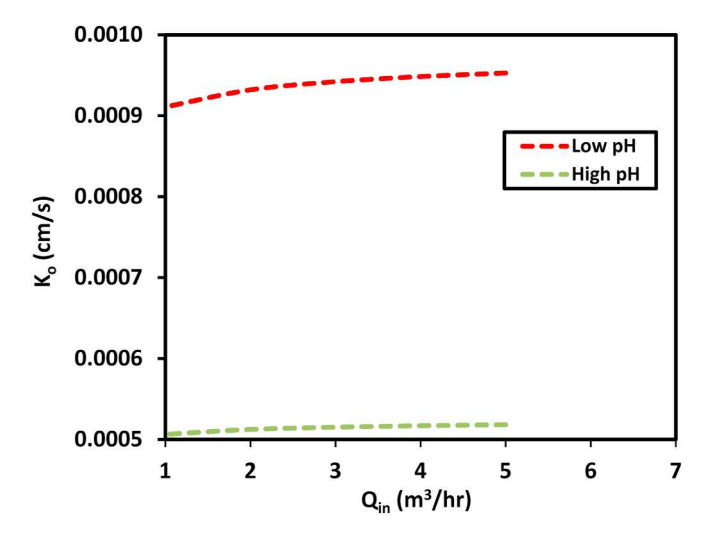


Fig. 12. Dependence of overall mass transfer coefficient of ammonia on feed volumetric flow rate for two modules in series.

rates on ammonia separation efficiency. Parallel to the trend reported earlier for experiments conducted in a much smaller module (i.e., MicroModule $^{\rm TM}$), our simulation illustrates a decrease in separation efficiency (i.e., -ln(1-E)) with the feed flow rate in Fig. 13a and b.

Fig. 13a and b also highlight the influence of strip side pH on NH₃ gas removal efficiency and the number of modules in series, n, required to achieve a certain level of concentration reduction from a feed level of 6000 ppm in once-through systems. For instance, our model suggests that the feed flow rate be set to 1 m³/h via one module at low H₂SO₄ solution pH and two modules at high strip side pH, in order to reduce the concentration of NH₃ in the effluent to 40 ppm i.e., (-ln(1-E) = 5). Such a comparison could be useful in making key decisions in industrial settings. In industries where the main aim is NH3 removal, a low H2SO4 solution pH would be favorable. Conversely, a high H₂SO₄ solution pH favors the production of ammonium sulfate which can be sold as fertilizer. Additional comparison made to the recirculation mode (Fig. 9) shows treatment times of about 60 min is required at low strip side pH, and 90 min at high pH to achieve the same results when the NH₃ feed solution is passed through two modules in series. Recirculation mode is optimal for lower feed volumes which may allow batch processing as well as better process control. On the other hand, once-through mode of operation with a larger number of modules becomes preferable for higher feed volumes without any consideration for the need of other ancillary equipment.

Another issue often comes up in any application of porous

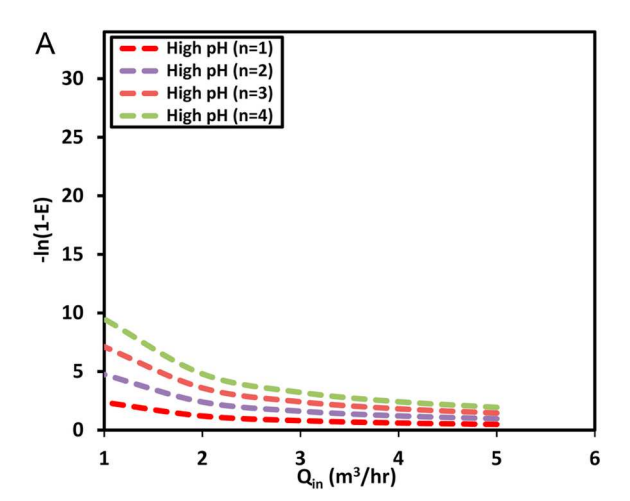


Fig. 13a. Once-through mode separation efficiency of ammonia exiting two modules in series as a function of feed volumetric flow rate for an incoming feed concentration of 6000 ppm ammonia; *strip-side* pH: *Low*.

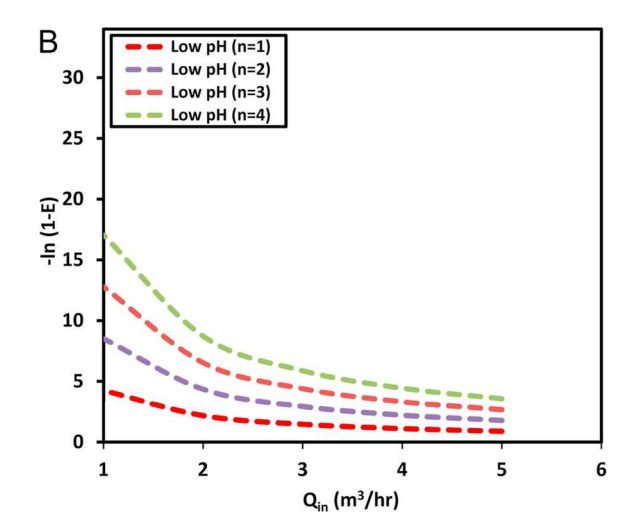


Fig. 13b. Once-through mode separation efficiency of ammonia exiting two modules in series as a function of feed volumetric flow rate for an incoming feed concentration of 6000 ppm ammonia; *strip-side* pH: *High*.

hydrophobic membranes with gas-filled pores namely, possible wetting of the membrane pores. The solution pH as such does not affect wetting of the membrane since the solution surface tensions continue to be quite high regardless of the pH. Unless the solution surface tension comes close to the critical surface tension of polypropylene, no wetting should take place. However, there are limited possibilities of surface modification of polypropylene by the acid and the base. The caustic strength is not very high at a pH of around 11; on the other hand, concentrated sulfuric acid strength is quite high. No information is available about wetting problems if any in such an application.

5. Concluding remarks

A resistances-in-series approach was used to successfully model ammonia removal behavior experimentally observed in a lab-scale crossflow module under higher pH conditions where strip side resistance comes into play. This model was then scaled-up and used to describe a batch-recirculation process-based ammonia removal from a large tank via two large 10x28 LiquiCel® modules connected in series. Both high strip-side pH and low strip-side pH conditions were modeled. A major aspect of the modeling involved accounting for water vapor transfer due to osmotic pressure difference between the feed solution and the strip solution; such transfer affects both feed and strip solutions considerably. Comparisons of the modeling results made with the results of a pilot-plant study gives reasonable insights into ammonia removal via these large devices. Continuous (once-through) ammonia removal was also briefly modeled to estimate the number of modules required for a given degree of ammonia removal with considerations of the effect of pH in the sulfuric acid-based strip solution.

Declaration of competing interest

The authors declare that they have no conflict of interest.

Acknowledgments

The authors gratefully acknowledge support for this research from the NSF Industry/University Cooperative Research Center for Membrane Science, Engineering and Technology that has been supported via two NSF Awards IIP1034710 and IIP-1822130. We are grateful to 3 M Corporation for donating a number of MicroModules™ to our research. Philip Aligwe was supported by Chemical and Materials Engineering at NJIT during 2019. Anu Alli's help to Philip Aligwe during the experiments is acknowledged.

Nomenclature

a, b, c Parameters/Constants in equation (6b)

 $a_{NH3/H2SO4}$ Stoichiometric coefficient of NH_3/H_2SO_4 in the acid-base reaction

 $egin{array}{ll} A_c & & & & & & \\ Membrane & cross-sectional area \\ A_{fc} & & & & & \\ Actual & flow & cross-sectional area \\ \end{array}$

 A_T Transfer area between two phases in the contactor C_{H2SO4} Initial sulfuric acid concentration on the strip side

 $\begin{array}{ll} C_o & \quad \text{Average ammonia inlet concentration} \\ C_{out} & \quad \text{Average ammonia outlet concentration} \\ C_t & \quad \text{Average tank concentration of ammonia} \\ d_i & \quad \text{Inner diameter of hollow fiber} \end{array}$

Outer diameter of hollow fiber

d_p Pore diameter

 d_F

D_{H2SO4,L} Diffusion coefficient of sulfuric acid in water

D_{NH3,L} Diffusion coefficient of ammonia in the bulk feed liquid

 $\begin{array}{ll} D_{NH3,g} & \text{Effective diffusion coefficient of NH}_3 \text{ gas through gas-filled pores} \\ D_{NH3,k} & \text{Knudsen diffusion coefficient of NH}_3 \text{ gas through gas-filled pores} \\ D_{H2O,k} & \text{Knudsen diffusion coefficient of H}_2\text{O gas through gas-filled pores} \\ \end{array}$

E NH₃ gas separation efficiency via the contactor

f_X Fractional open area for flow of liquid (in the radial plane, inward or outward) in large module

f_p Packing fraction of hollow fibers in large module

G Total rate of NH₃ transfer

h Contribution factor of ionic/gaseous species in solution towards the effective Henry's constant

H Henry's constant in H₂O

H_{eff} Effective Henry's constant in H₂O

I₁ Ratio of inlet to outlet ammonia concentrations leaving one zone of a contactor at low H₂SO₄ solution pH conditions, defined by eq. (18c)
I₂ Ratio of inlet to outlet ammonia concentrations leaving one zone of a contactor at high H₂SO₄ solution pH conditions, defined by eq. (23a)

 J_{H2O} Molar flux of water

 $\begin{array}{ll} k_f & \quad \text{Feed mass transfer coefficient} \\ k_m & \quad \text{Membrane mass transfer coefficient} \end{array}$

K_o Overall mass transfer coefficient of ammonia

K'H2O Liquid phase volume flux of water

L Effective hollow fiber length in the module

MW_{H2O} Molecular weight of water MPE Mean percent error

n_f Number of fiber layers in crossflow direction

N Total number of hollow fibers

PI Phase interface

 $\begin{array}{ll} P_f & \quad & \text{Feed side water vapor pressure} \\ P_s & \quad & \text{Strip side water vapor pressure} \end{array}$

 $\begin{array}{ll} Q_{in} & \quad & \text{Inlet volumetric flow rate of ammonia feed solution} \\ Q_{loss} & \quad & \text{Volumetric flow rate due to water vapor transport} \\ Q_{out} & \quad & \text{Outlet volumetric flow rate of ammonia feed solution} \end{array}$

 $\begin{array}{lll} r & Radius \ of \ differential \ slice \\ R_{ci} & Inner \ radius \ of \ cartridge \\ R_{co} & Outer \ radius \ of \ cartridge \\ R_i & Inner \ radius \ of \ hollow \ fiber \\ R_o & Outer \ radius \ of \ hollow \ fiber \\ R & Universal \ gas \ constant \\ RF & Reaction \ front \end{array}$

RF Reaction from t Process time T Temperature

v Axial velocity through the bore/lumen of a hollow fiber v_r Local radial velocity on the shell side at radius r v_x Local axial velocity on the shell side at distance x

V Feed tank volume at time t V_o Initial feed tank volume

 ΔV_f Change in tank ammonia solution volume

W Length of hollow fiber perpendicular to feed solution in cross flow Vertical location of ammonia concentration in the module

δ Hollow fiber membrane thickness

Membrane porosity

 Λ Composite transport property parameter, defined by eq. (6b)

 Φ Enhancement factor for k_s in an instantaneous acid-base reaction, eq. (9)

 ρ_{NH3} Density of ammonia in the bulk feed solution

 $\begin{array}{ll} \rho_{H2O} & \text{Density of liquid water} \\ \tau & \text{Membrane tortuosity} \\ \mu & \text{Viscosity of liquid} \end{array}$

Other notations (subscripts)

b Bulk
f Feed
i Interface
m Membrane
n Ammonia
s Strip

Appendix A. Concentration decrease in strip-side sulfuric acid

The molar flux of water, $J_{H,O}$ can be calculated from its Knudsen diffusion coefficient, $D_{H2O,K}$ as follows:

$$J_{H_2O} = \frac{D_{H_2O,k}\left(\frac{\varepsilon}{\varepsilon}\right)}{\delta RT} * P_f = \frac{7.8955 * 10^{-6} \left(\frac{m^2}{s}\right) * \frac{0.4}{6.4}}{4 * 10^{-5} (m) * 8.3145 \left(\frac{P_2 - m^3}{K - mol}\right) * 298K} * 3156.5(Pa) = 1.57 * 10^{-6} \frac{mol}{cm^2 - s}$$
(A1)

Subsequently, the liquid phase volume flux of water, K'_{H_2O} , is given by the following expression and calculated as follows:

$$\dot{K}_{H_2O} = J_{H_2O} * \frac{MW_{H_2O}}{\rho_{H_2O}} = 1.57*10^{-6} \left(\frac{mol}{cm^2 - s}\right) * \frac{18\left(\frac{g}{mol}\right)}{1\left(\frac{g}{cm^3}\right)} = 2.8275*10^{-5} \frac{cm}{s}.$$
(A2)

Hence, the rate of water vapor loss, Q_{loss} is given by

$$Q_{loss} = K^*_{H_2O} * A_T = 2.8275 * 10^{-5} \left(\frac{cm}{s}\right) * 2,600,000 cm^2 * \frac{1(m^3)}{100^3 (cm^3)} * \frac{3600s}{1hr} = 0.26 \frac{m^3}{hr}$$
(A3)

Therefore, a total of $0.52m^3$ of water vapor is transferred to the strip tank during the entire operation (i.e., t = 2 h). This calculation assumes no change during the process. In fact, transfer of water vapor to the strip solution will increase its water vapor pressure and continue to reduce the rate of water vapor transfer. Therefore, the expected water vapor transfer will be significantly lower.

From [24], the initial sulfuric acid concentration $C_{H2SO4|_{t=0}}$, and fill volume of the sulfuric acid in the strip tank V_i , are reported to be 98% and 0.12 m³ respectively. Therefore, if we assumed unchanged mode of operation, using the molar balance equation, the final sulfuric acid concentration $C_{H2SO4|_{t=2hrs}}$ can be estimated as follows:

$$C_{H2SO4|t=2hrs} = \frac{C_{H2SO4|t=0} * V_i}{(V_i + 0.52)} = \frac{98\% * 0.12m^3}{0.64m^3} = 18.4\%$$
(A4)

In reality, the concentration will be higher. Further, the temperature of this strip solution is also important as there is some heat exchange going on with the feed solution in the membrane modules as well as with the strip tank environment and reaction enthalpy generated by the exothermic acid-base reaction.

References

- [1] J. Plautz, Piercing the haze, Science 361 (Issue 6407) (2018) 1060–1063.
- [2] F. Ozyonar, B. Karagozoglu, M. Kobya, Air stripping of ammonia from coke wastewater, Int. J. Eng. Sci. Technol. 15 (2012) 85–91.
- [3] J.M. Wright, W.T. Lindsay Jr., T.R. Druga, USAEC Comm. R&D Report WAPD TM-204, 1961, p. 32.
- [4] C.N. Sawyer, P.L. McCarty, G.F. Parkin, Chemistry for Environmental Engineering and Science, fifth ed., McGraw-Hill Education, New York, NY, 2002.
- [5] J.L. Campos, J.M. Garrido-Fernandez, R. Mendez, J.M. Lema, Nitrification at high ammonia loading rates in an activated sludge unit, Bioresour. Technol. 68 (2) (1999) 141–148.
- [6] T.C. Jorgensen, L.R. Weatherley, T.C. Jorgensen, L.R. Weatherley, Ammonia removal from Wastewater by ion exchange in the presence of organic contaminants, Water Res. 37 (2003) 1723–1728.
- [7] M. Imai, S. Furusaki, T. Miyauchi, Separation of volatile materials by gas membranes, I&EC Proc. Des. and Dev. 21 (1982) 421–426.
- [8] Zhang Qi, E.L. Cussler, Hollow fiber gas membranes, AIChE J. 31 (1985)
- [9] M.J. Semmens, D.M. Foster, E.L. Cussler, Ammonia removal from water using microporous hollow fibers, J. Membr. Sci. 51 (1990) 127.
- [10] C.F. Kenfield, R. Qin, M.J. Semmens, E.L. Cussler, Cyanide recovery across hollow fiber gas membranes, Environ. Sci. Technol. 22 (1989) 1151–1155.

- [11] A.E. Short, S.F. Haselmann, M.J. Semmens, The GM-IX process: a pilot study for recovering zinc cyanides, J. Environ. Sci. Heal. Part a-Environ. Sci. Eng. Toxic Hazard. Subst. Control. 32 (1997) 215–239.
- [12] Y.J. Qin, J.M.S. Cabral, S.C. Wang, Hollow-fiber gas-membrane process for removal of $\rm NH_3$ from solution of $\rm NH_3$ and $\rm CO_2$, AIChE J. 42 (1996) 1945–1956.
- [13] J. He, H. Liu, P. Shan, K. Zhang, Y. Qin, L. Liu, Supported-gas-membrane process for removal and recovery of aliphatic amines from aqueous streams, Chem. Eng. Sci. 141 (2016) 330–341.
- [14] TB 74, 2009; TB 84, Membrana, Charlotte, NC, USA, 2015.
- [15] H. Estay, M. Ortiz, J. Romero, A novel process based on gas filled membrane absorption to recover cyanide in gold mining, Hydrometallurgy 134–135 (2013) 166–175.
- [16] H. Estay, E. Troncoso, J. Romero, Design and cost estimation of a gas-filled membrane absorption (GFMA) process as alternative for cyanide recovery in gold mining, J. Membr. Sci. 466 (2014) 253–264.
- [17] H. Estay, E. Troncoso, R. Ruby-Figueroa, J. Romero, Performance evaluation of mass transfer correlations in the GFMA process: a review with perspectives to the design. J. Membr. Sci. 554 (2018) 140–155.
- [18] H. Estay, E. Troncoso, R. Ruby-Figueroa, J. Romero, Assessment of industrial modules to design a GFMA process for cyanide recovery based on a phenomenological model performance evaluation of mass transfer correlations in the GFMA process: a review with perspectives to the design, Processes 6 (4) (2018) 34. https://doi.org/10.3390/pr6040034.
- [19] Z. Shen, B. Han, S.R. Wickramasinghe, Cyanide removal from wastewater using gas membranes: commercial scale study, Water Environ. Res. 76 (1) (2004) 15–22.

- [20] B. Han, Z. Shen, S.R. Wickramasinghe, Cyanide removal from industrial wastewaters using gas membranes, J. Membr. Sci. 257 (1–2) (2005) 171–181.
- [21] B. Han, Z. Shen, S.R. Wickramasinghe, Fouling and cleaning of gas membranes for cyanide removal, Separ. Sci. Technol. 40 (6) (2005) 1169–1180.
- [22] J. Shen, B. Han, S.R. Wickramasinghe, Cyanide removal from industrial praziquantel wastewaters using integrated coagulation–gas-filled membrane absorption process, Desalination 195 (1–3) (2006) 40–50.
- [23] Z. Shen, L. Zhang, S. Mondal, S.R. Wickramasinghe, Suppression of osmotic distillation in gas membrane processes, Separ. Sci. Technol. 43 (15) (2008) 3813–3825.
- [24] M. Ulbricht, G. Lakner, J. Lakner, K. Belafi-Bako, TransMembraneChemiSorption of ammonia from sealing water in Hungarian powder metallurgy furnace, Desalination and Water Treatment 75 (2017) 253–259.
- [25] W.S.W. Winston, K.K. Sirkar (Eds.), Reprinted, Membrane Handbook, Chap. 38, Van Nostrand Reinhold, Kluwer Academic, New York, 1992, 2001; Springer, 2012.
- [26] P.R. Danesi, L. Reichley-Yinger, P.G. Rickert, Lifetime of supported liquid membranes: the influence of interfacial properties, chemical composition and water transport on the long- term stability of the membranes, J. Membr. Sci. 31 (1987) 117–145.
- [27] P.A. Aligwe, K.K. Sirkar, C.J. Canlas, Hollow fiber gas membrane-based removal and recovery of ammonia from water in three different scales and types of modules, Separ. Purif. Technol. 224 (2019) 580–590.

- [28] A. Sengupta, P.A. Peterson, B.D. Miller, J. Schneider, C.W. Fulk Jr., Large-scale application of membrane contactors for gas transfer from or to ultrapure water, Separ. Purif. Technol. 14 (1998) 189–200.
- [29] J.-M. Zheng, Z.-W. Dai, F.-S. Wong, Z.-K. Xu, Shell side mass transfer in a transverse flow hollow fiber membrane contactor, J. Membr. Sci. 261 (2005) 114–120.
- [30] K.K. Sirkar, Separation of Molecules, Macromolecules and Particles: Principles, Phenomena and Processes, Cambridge University Press, 2014. Ch. 5.3.1.
- [31] J.I. Gmitro, T. Vermeulen, Vapor-liquid equilibria for aqueous sulfuric acid, AIChE J. 10 (5) (1964) 740–746.
- [32] J.S. Mackie, P. Meares, The diffusion of electrolytes in a cation-exchange resin membrane I. Theoretical, Proc. Roy. Soc. Lond. A 232 (1191) (1955) 498–509.
- [33] P. Schöner, P. Plucinski, W. Nitsch, U. Daiminger, Mass transfer in the shell side of cross flow hollow fiber modules, Chem. Eng. Sci. 53 (13) (1998) 2319–2326.
- [34] A. Baudot, J. Floury, H.E. Smorenburg, Liquid-liquid extraction of aroma compounds with hollow fiber contactor, AIChE J. 47 (8) (2001) 1780–1793.
- [35] J. Choi, M. Cui, Y. Lee, J. Ma, J. Kim, Y. Son, J. Khim, Hybrid reactor based on hydrodynamic cavitation, ozonation, and persulfate oxidation for oxalic acid decomposition during rare-earth extraction processes, Ultrason. Sonochem. 52 (2019) 326–335.